Journal for ImmunoTherapy of Cancer

Integrated analysis of tertiary lymphoid structures and immune infiltration in ccRCC microenvironment revealed their clinical significances: a multicenter cohort study

Yu-Qi Wang,[1] Wen-Jin Chen,[1,2] Wang Zhou,[1] Ke-Qin Dong,[1,3] Li Zuo,[4] Da Xu,[2] Jia-Xin Chen,[1,2] Wei-Jie Chen,[2] Wen-Yan Li,[1] Zi-Chang Liu,[1] Zheng-Yu Jiang,[5] Yi-Fan Tang,[6] Yu-Xuan Qin,[1] Lin-Hui Wang,[7] Xiu-Wu Pan,[1] Xin-Gang Cui [1]

To cite: Wang Y-Q, Chen W-J, Zhou W, *et al*. Integrated analysis of tertiary lymphoid structures and immune infiltration in ccRCC microenvironment revealed their clinical significances: a multicenter cohort study. *Journal for ImmunoTherapy of Cancer* 2024;**12**:e008613. doi:10.1136/jitc-2023-008613

► Additional supplemental material is published online only. To view, please visit the journal online (https://doi.org/10.1136/jitc-2023-008613).

Y-QW, W-JC, WZ, K-QD and LZ contributed equally.

Accepted 02 June 2024

For numbered affiliations see end of article.

Correspondence to
Dr Xin-Gang Cui;
cuixingang@xinhuamed.com.cn

Dr Xiu-Wu Pan;
panxiuwu@126.com

Dr Lin-Hui Wang;
wanglinhui@smmu.edu.cn

ABSTRACT

Background Tertiary lymphoid structures (TLSs) serve as organized lymphoid aggregates that influence immune responses within the tumor microenvironment. This study aims to investigate the characteristics and clinical significance of TLSs and tumor-infiltrating lymphocytes (TILs) in clear cell renal cell carcinoma (ccRCC).

Methods TLSs and TILs were analyzed comprehensively in 754 ccRCC patients from 6 academic centers and 532 patients from The Cancer Genome Atlas. Integrated analysis was performed based on single-cell RNA-sequencing datasets from 21 ccRCC patients to investigate TLS heterogeneity in ccRCC. Immunohistochemistry and multiplex immunofluorescence were applied. Cox regression and Kaplan-Meier analyses were used to reveal the prognostic significance.

Results The study demonstrated the existence of TLSs and TILs heterogeneities in the ccRCC microenvironment. TLSs were identified in 16% of the tumor tissues in 113 patients. High density (>0.6/mm^2) and maturation of TLSs predicted good overall survival (OS) (p<0.01) in ccRCC patients. However, high infiltration (>151) of scattered TILs was an independent risk factor of poor ccRCC prognosis (HR=14.818, p<0.001). The presence of TLSs was correlated with improved progression-free survival (p=0.002) and responsiveness to therapy (p<0.001). Interestingly, the combination of age and TLSs abundance had an impact on OS (p<0.001). Higher senescence scores were detected in individuals with immature TLSs (p=0.003).

Conclusions The study revealed the contradictory features of intratumoral TLSs and TILs in the ccRCC microenvironment and their impact on clinical prognosis, suggesting that abundant and mature intratumoral TLSs were associated with decreased risks of postoperative ccRCC relapse and death as well as favorable therapeutic response. Distinct spatial distributions of immune infiltration could reflect effective antitumor or protumor immunity in ccRCC.

WHAT IS ALREADY KNOWN ON THIS TOPIC

⇒ Tertiary lymphoid structures (TLSs) are present in multiple tumors and regarded as predictors for evaluating clinical prognosis, but the mechanism of TLSs is not shown for prognostication of clear cell renal cell carcinoma (ccRCC) patients.

WHAT THIS STUDY ADDS

⇒ The study demonstrated the clinical significance of heterogeneous TLSs and immune infiltration in ccRCC, based on multicenter study cohorts. Mature TLSs were identified and correlated with good outcomes and therapeutic responses. Immune cell senescence associated with TLS development was elucidated using a single cell sequencing platform.

HOW THIS STUDY MIGHT AFFECT RESEARCH, PRACTICE OR POLICY

⇒ The study proposed that mature TLSs may be involved in modulating immune populations to influence the strength of tumor-specific immune responses and could be exploited in future therapeutic interventions for ccRCC.

INTRODUCTION

Renal cell carcinoma (RCC) accounts for about 85%–90% of all primary kidney malignancies, of which clear cell RCC (ccRCC) is the most common type and also one of the leading causes of cancer-related deaths.[1 2] According to the latest guidelines, the updated Tumor Node Metastasis (TNM) classification system is recommended for the evaluation and treatment of RCC.[3] However, significant differences in the clinical outcomes of patients diagnosed with the same pathological classification and stage have been observed clinically, potentially correlated with the different tumor immune environment.[4] ccRCC displays a wide spectrum of

immune cell infiltration patterns and clinical behaviors. As a group of heterogeneous immunogenic neoplasms with a wide spectrum of immune cell infiltration patterns and clinical behaviors, the intricate immune infiltration of ccRCC within the tumor microenvironment (TME) is incompletely characterized.

Evidence implicates complex interactions between tumor cells and immune cells,[5] with the host immune system and tumor processes constantly interacting to influence tumor progression.[6 7] Extensive studies have shown the critical roles of infiltrated immune cells in regulating tumor progression and patient survival, forming an ecosystem within the TME.[6 8 9] Therefore, an exploration of the immune contexture of the TME may provide further insights into the prognosis of ccRCC. In recent years, new cutting-edged immunotherapies for solid tumors have emerged. But the limited response efficacy in current ccRCC treatment with these immunotherapies underscores the need to gain a better understanding about the immunobiology of kidney neoplasms. More recent studies[10] highlight the presence of tumor-associated tertiary lymphoid structures (TLSs) as an analog of second lymphoid organs. Studies have demonstrated their nonnegligible roles in the immune microenvironment as providers of an important milieu for immune response and mediators of antitumor immunity.[11–14] TLSs vary in their composition, density, maturation state and spatial distribution, indicating the existence of certain heterogeneities in TLSs; for instance, mature TLSs are composed of a $CD20^+$B cell follicle with a core germinal center (GC) area surrounded by plasma cells juxtaposing a $CD3^+$T cell-rich zone, making up the bulk of TLS-associated immune cells. TLSs arise in response to immunological stimuli,[15] representing privileged sites where tumor antigens nearby can be presented to T cells by dendritic cells, as well as the activation, proliferation and differentiation of T and B cells. This process helps develop effector memory T helper cells and cytotoxic cells, memory B cells and antibody-producing plasma cells.[16] Both humoral and cell-mediated immune responses can be generated or boosted within this structure. TLSs could also facilitate integrated antitumor responses within the TME by combining the actions of tumor-infiltrating plasma cells and cytotoxic T cells.[17]

TLSs are associated with a favorable prognosis in a number of cancer types, although with some contradicting results.[12] In the study of ccRCC, spatial transcriptomics analysis of TLSs in RCC recognized them as sites of in situ B cell maturation, and the presence of IgG-stained tumor cells correlated with enhanced therapeutic responses and longer progression-free survival (PFS) in patients.[18] Multiomic data also supported the role of B cells and TLSs in response to immune checkpoint inhibitors in metastatic RCC patients.[12] Nonetheless, the characteristics and detailed underlying mechanisms of TLSs in ccRCC still remain elusive. There is a lack of large cohort studies and the correlation analysis between TLSs and tumor-infiltrating lymphocytes (TILs) of ccRCC. The contrasting roles of TLSs which behave as a double-edged sword in the host–tumor interaction indicated that a better appreciation of TLSs function and contribution would be essential to maximize their therapeutic targets. Here, a reliable and prudent evaluation system as well as an exploration of the TLSs heterogeneity could clarify the characteristics of TLSs accurately and conclusively.

The aim of this study was to comprehensively evaluate the composition, abundance and maturity states of TLSs based on a large multicenter cohort and single-cell RNA-sequencing (scRNA-seq) analysis. We evaluated the positive prognostic effect of high-TLS density and mature state. Furthermore, we elaborated the negative effect of TILs in the TME of ccRCC, uncovering the opposite effect between different properties of immune spatial distribution. Additionally, we elucidated age-associated TLSs in cohort patients and assessed at single cell resolution that immature TLS displayed the property of cell senescence. Collectively, our results indicated the roles of intratumoral immune context with TLSs and TILs and the correlation with aging in the TME of ccRCC with the aim of providing new insights into how they affect clinical prognosis and therapeutic response of ccRCC patients.

METHODS

Patient cohort and tissue samples

We retrospectively collected 754 patients pathologically diagnosed with ccRCC from 6 independent academic centers: Xinhua Hospital (Shanghai, China), the Third Affiliated Hospital of Second Military Medical University (Shanghai, China), Changhai Hospital of the Second Military Medical University (Shanghai, China), Changzhou No.2 People's Hospital (Changzhou, China), the First Affiliated Hospital of Wannan Medical College (Wuhu, China), and Taizhou First People's Hospital (Taizhou, China). Naïve cohort (n=720): these patients received either radical or partial nephrectomy from 2010 to 2018 with available RCC tissue microarrays retrieved. Detailed characteristics of the cohorts are presented in online supplemental tables S1, S2 and figure S1. We abstracted data on relevant clinicopathologic covariates including age at surgery, gender, TNM stage, WHO/International Society of Urologic Pathologist (WHO/ISUP) grade, T categories, presence of necrosis, sarcomatoid components, cystic architecture, multifocality, and tumor size. The primary endpoint for the current study was overall survival (OS), which was defined as the time from diagnosis to death or the last follow-up date. In addition, a set of sample data of ccRCC patients were obtained from The Cancer Genome Atlas (TCGA, https://portal.gdc.cancer.gov) cohort. Treatment cohort (n=34): these patients who treated with antiangiogenic tyrosine kinase inhibitor (TKI) or TKI/immune checkpoint blockade (ICB) combination therapy were enrolled with evaluable response to treatment. Tumor assessments were performed according to Response Evaluation Criteria in Solid Tumors V.1.1.

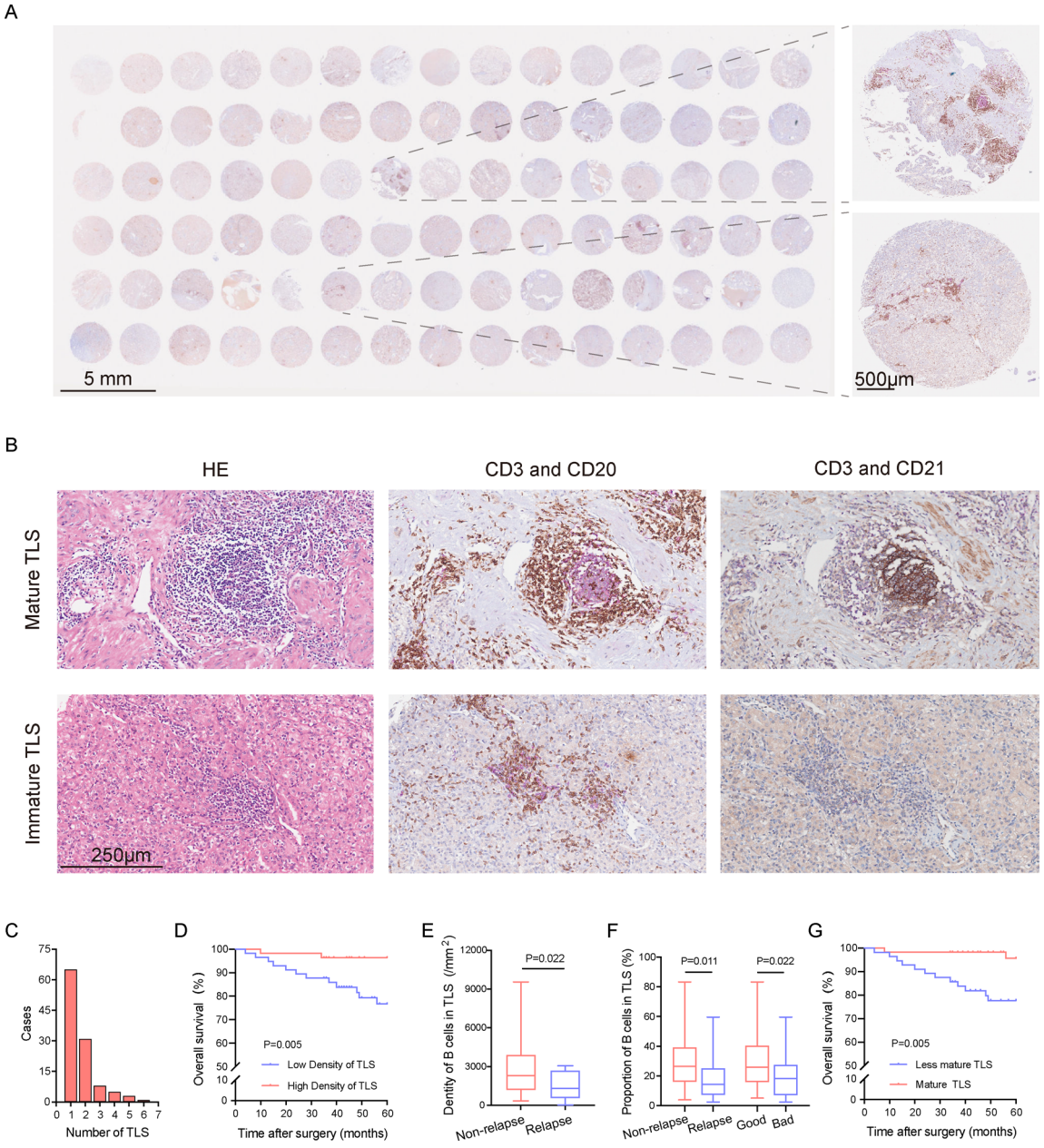

Figure 1 The expression characteristics of TLSs in retrospectively collected ccRCC tissue microarrays. (A) Thumbnail of tumor microarray, showing the expression of TLSs in ccRCC. Scale bar, 5 mm and 500 μm; (B) Representative figures of TLSs in ccRCC. Scale bar, 250 μm; (C) Number of TLSs in ccRCC cases; (D) Association between TLS density and OS (p=0.005); (E) Density of TLSs in non-relapse and relapse groups (p=0.022); (F) Proportion of B cells within TLSs in non-relapse and relapse groups (p=0.011); good and bad outcome groups (p=0.022); (G) Association between TLSs maturity and OS (p=0.005). ccRCC, clear cell renal cell carcinoma; OS, overall survival; TLSs, tertiary lymphoid structures.

Immunohistochemistry and multiplex immunofluorescence examination

Five μm thick tissue sections were cut from formalin-fixed paraffin-embedded specimens. The ccRCC samples were included in tissue microarrays. H&E staining was conducted to examine the histopathological records of unspecific lymphocyte infiltration. Immunohistochemistry (IHC) was performed on all cases with CD3 combined with CD20 and CD3 combined with CD21. Stainings were performed according to the manufacturer's recommendations. The microarray slides were incubated overnight with antibodies against CD3 (ab237721, rabbit anti-human polyclonal, 1:1000; Abcam) and CD20 (KIT-0001, mouse anti-human polyclonal, 1:100) at 4°C in an incubator for costaining.

Multiplex immunofluorescence (mIF) was performed according to the manufacturer's protocol using PANO 7-plex IHC kit (Panovue). The slides were sequentially applied with primary antibodies of two panels, including CD3, CD4, CD8, CD20, CD21 and CD56; CD3, CD20, CD21, CD31, CD68 and CD163 (online supplemental table S3), followed by corresponding horseradish

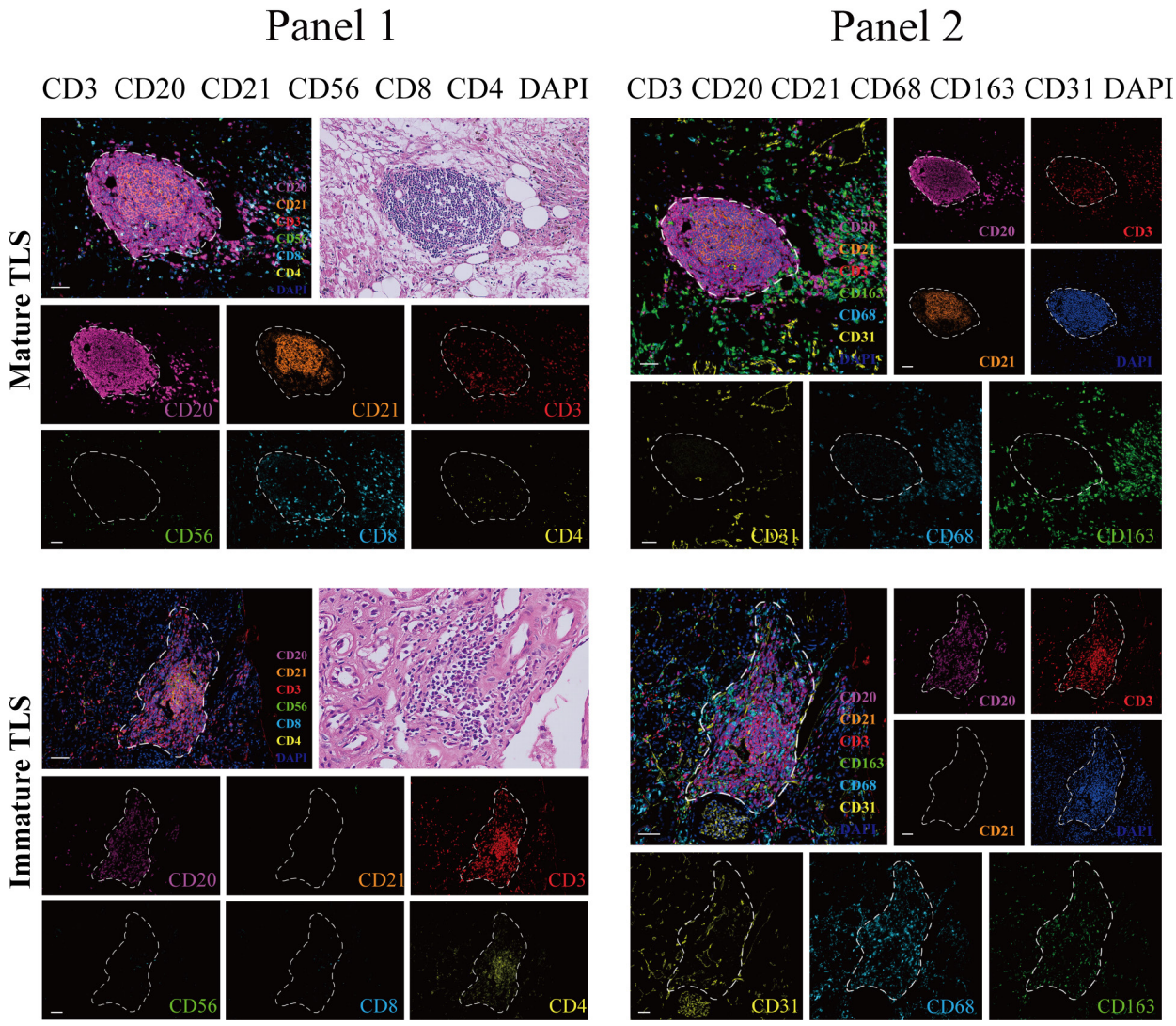

Figure 2 Evaluation of TLSs in ccRCC using multiplex immunofluorescence. The staining images combining CD3 (red), CD8 (cyan), CD4 (yellow), CD21 (orange), CD56 (green) and CD20 (magenta) in one tissue session and CD3 (red), CD68 (cyan), CD31 (yellow), CD21 (orange), CD163 (green) and CD20 (magenta) in another serial section. TLSs are circled with dotted white lines. Scale bars, 50 µm. ccRCC, clear cell renal cell carcinoma; TLSs, tertiary lymphoid structures.

peroxidase-conjugated secondary antibody incubation and tyramide signal amplification. Nuclei were stained with 4'–6'-diamidino-2-phenylindole (Sigma-Aldrich) after labeling all human antigens. Subsequently, the slides were scanned and imaged using the Olympus vs200 scanner (Olympus Germany) coupled with the Olympus UPLXAPO 20× objective lens.

TLS identification and evaluation

TLSs were morphologically recognized as ectopic lymphoid aggregates showing distinct B cell zones and T cell zones. GC-positive was considered if at least one TLS showed morphology of proliferating centroblasts. To further characterize the maturation of TLSs, mIF using a 9-antibody system was carried out, in which mature TLSs presented with dense lymphocyte aggregates and immune cell infiltration. The expression of CD21 is vital for mature B cells and follicular dendritic cells in TLSs, and positive CD31 staining indicates vascularization within TLS areas.[19] The TLS maturity score=TLS proportion (defined as the ratio of TLS area to total tissue area)×immunopositivity score, which ranges from 0 to 300. In tumor tissues with more than one TLS, the maturity score was identified based on the most mature TLS. Two experienced pathologists independently assessed the staining for the presence, maturation and pattern of expression according to standard procedures.

An IHC scoring system was established for TILs evaluation. Lymphocyte density was calculated as densities of cells expressing a given marker within the tumor region. The immunopositivity of B and T cells was evaluated by the percentage of area covered by positive cells with an overall IHC score from 0 to 150. Similarly, the overall TILs score of 0–300 was generated simultaneously for evaluation. All specimens underwent pathological examination and quantitative image analysis. Automatic quantification of positive stained nuclei count and the TLSs

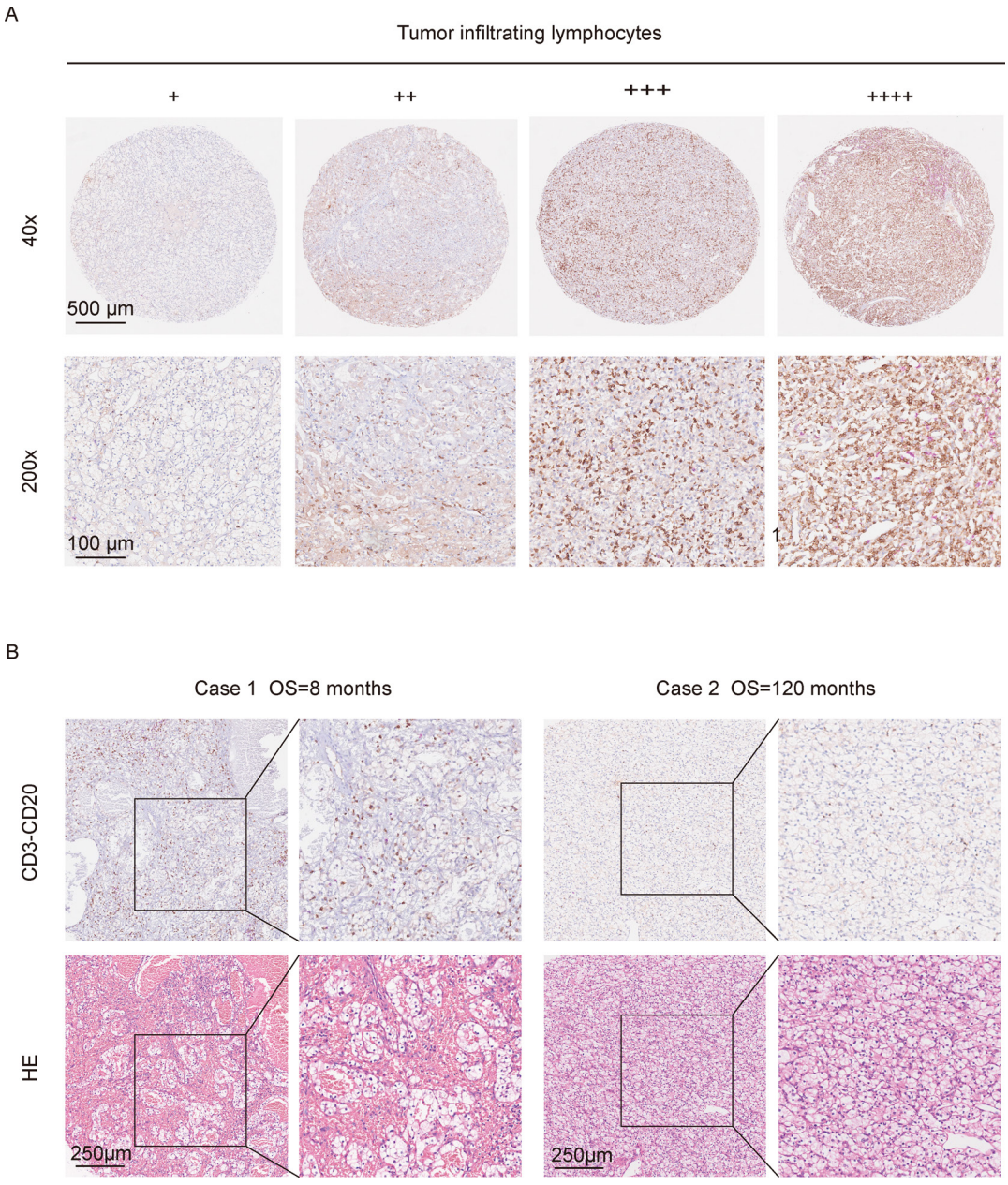

Figure 3 Distinct expression of TILs in ccRCC tissue samples. (A) Detection of TILs expression levels in ccRCC by CD3 and CD20 immunochemistry. Scale bar, 500 μm and 100 μm; (B) The representative figures of TILs expression in patients with different OS. Scale bar, 250 μm. ccRCC, clear cell renal cell carcinoma; OS, overall survival; TILs, tumor-infiltrating lymphocytes.

area annotation of the staining images were carried out using QuPath V.0.2.3.[20] Cell classification was visually verified to have occurred correctly.

Single-cell RNA-seq data processing

We collected single cell RNA datasets of 21 ccRCC patients from our cohort and previous studies.[21] Single cells from 15 ccRCC patients in our cohort were selected using a microfluid system based on 10×Genomics platform. Cell Ranger software was applied to identify quantitative of the original data. Cell filtration and data quality control were done through Seurat (V.4.1.1). To remove low-quality cells, cells with fewer than 200 or more than 5000 genes, or with mitochondrial genes exceeding 30% were depleted. Cell cycle genes were annotated using the cc.genes.updated.2019 version. Cell cycle scores were computed using the Cyclone package (V.1.18.1), incorporating variables "S.Score" and "G2M.Score" during standardization. Doublet cell identification and removal were conducted using the DoubletFinder package (online supplemental figure S5). Identification of 2000 highly variable genes was accomplished through the "FindVariableGenes" function. Principal component analysis (PCA) was applied to the single-cell expression matrix using the "RunPCA" function. The top 30 principal components were employed for clustering via the Louvain graph-clustering methodology. The batch effect from different

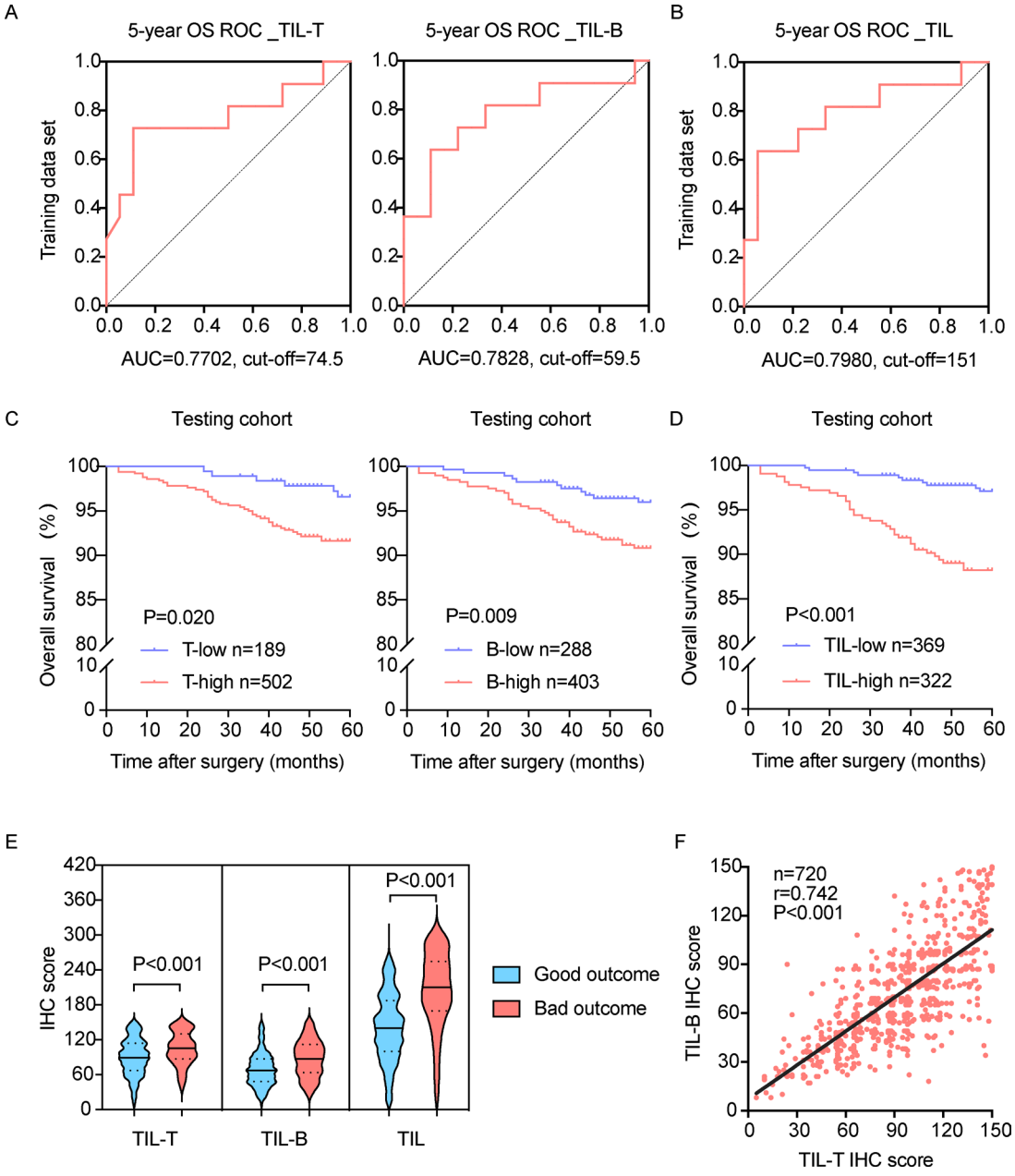

Figure 4 The correlation between TILs and clinical outcomes in ccRCC patients. (A) ROC curves of TIL-T (AUC=0.7702, cut-off=74.5) and TIL-B (AUC=0.7828, cut=off=59.5) in the training cohort; (B) ROC curve of TILs (AUC=0.798, cut-off=151) in the training cohort; (C) Kaplan-Meier survival curves of TIL-T (p=0.02) and TIL-B (p=0.009) in the testing cohort; (D) Kaplan-Meier survival curve of TILs in the testing cohort (p<0.001); (E) Violin plots of the IHC score of TIL-T (p<0.001), TIL-B (p<0.001), TIL (p<0.001) in different outcome groups; (F) The scatter diagram shows the correlation between TIL-T and TIL-B (r=0.742, p<0.001). AUC, area under curve; ccRCC, clear cell renal cell carcinoma; IHC, immunohistochemistry; ROC, receiver operation curve; TILs, tumor-infiltrating lymphocytes; TLSs, tertiary lymphoid structures.

samples was eliminated using "Runharmony" by running the align_cds() function (https://github.com/immunogenomics/harmony). Marker genes were screened using "FindAllMarker" function. Cell type markers to identify different cell clusters were selected from previous studies and CellMarker website.

Gene expression analysis

Differentially expressed genes (DEGs) were calculated using the "FindMarker" function of Seurat Package. A threshold of logFC 0.2 was applied, which was visualized in a volcano map. P values less than 0.05 were considered statistically significant. Subsequently, for B cell populations subgrouped by Monocle3, we mapped the grouping information back to the Seurat object and calculated the differential genes that rewrite the grouping information. The protein interaction network was performed using the protein–protein interactome (PPI) and transcriptional factor-gene (TF-gene) interaction of gene regulation networks. The generic PPI used parameters from the STRING interactome, with a confidence score cut-off

Table 1 Influencing factors of overall survival and progression-free survival of ccRCC patients among clinical characteristics and tumor-infiltrating lymphocytes of patients with ccRCC in the naïve cohort (n=720)

			OS				PFS			
			Outcome	Average survival			Outcome	Average survival		
Characteristics, n (%)		Total (n=720)	(death)	(month)	χ^2	P value	(recurrence)	(month)	χ^2	P value
Age	≤65 years	549 (76.3)	34 (53.1)	58.051	21.151	<0.001	44 (57.1)	57.28	18.648	<0.001
	>65 years	171 (23.7)	30 (46.9)	54.3			33 (42.9)	52.78		
Gender	Male	497 (69)	48 (75)	56.922	1.127	0.289	58 (75.3)	55.891	1.632	0.201
	Female	223 (31)	16 (25)	57.679			19 (24.7)	56.933		
WHO/ISUP	I and II	623 (86.5)	35 (54.7)	58.162	67.047	<0.001	45 (58.4)	57.655	68.893	<0.001
	III and IV	97 (13.5)	29 (45.3)	50.689			32 (41.6)	46.992		
TNM stage	1	623 (86.5)	33 (51.6)	58.34	90.394	<0.001	38 (49.3)	58.026	140.211	<0.001
	2	38 (5.3)	9 (14.1)	52.06			11 (14.3)	48.943		
	3 and 4	59 (8.2)	22 (34.4)	47.956			28 (36.4)	41.639		
T stage	T1	619 (86)	31 (48.4)	58.411	96.53	<0.001	37 (48)	58.073	130.619	<0.001
	T2	31 (4.3)	8 (12.5)	51.993			10 (13)	48.158		
	T3 and T4	70 (9.7)	25 (39.1)	57.156			30 (39)	43.244		
Necrosis	Absent	598 (83.1)	37 (57.8)	58.042	33.225	<0.001	43 (55.8)	57.55	50.009	<0.001
	Present	122 (16.9)	27 (42.2)	52.831			34 (44.2)	49.624		
Sarcoma	Absent	712 (98.9)	62 (96.9)	57.243	2.902	0.088	73 (94.8)	56.394	17.009	<0.001
	Present	8 (1.1)	2 (3.1)	49.375			4 (5.2)	40.625		
Cystic	Absent	581 (80.7)	58 (90.6)	56.869	4.341	0.037	68 (88.3)	56.011	3.063	0.08
	Present	139 (19.3)	6 (9.4)	58.351			9 (11.7)	57.065		
Multifocality	Absent	695 (96.5)	56 (87.5)	57.438	19.283	<0.001	68 (88.3)	56.546	21.361	<0.001
	Present	25 (3.5)	8 (12.5)	49.393			9 (11.7)	46.925		
Size	≤4 cm	464 (64.4)	19 (29.7)	58.782	37.152	<0.001	23 (29.9)	58.577	47.166	<0.001
	>4 cm	256 (35.6)	45 (70.3)	54.23			54 (70.1)	51.946		
TLS density	No TLS	607 (84.3)	50 (78.1)	57.391	14.14	0.001	64 (83.1)	56.346	8.46	0.015
	Low density	57 (7.9)	12 (18.8)	53.141			11 (14.3)	52.013		
	High density	56 (7.8)	2 (3.1)	58.643			2 (2.6)	59.039		
TLS maturity	No TLS	607 (84.3)	50 (78.1)	57.391	11.049	0.004	64 (83.1)	56.346	3.474	0.176
	Less mature	54 (7.5)	11 (17.2)	52.737			9 (11.7)	52.664		
	Mature	59 (8.2)	3 (4.7)	58.78			4 (5.2)	58.106		

Continued

Table 1 Continued

Characteristics, n (%)		Total (n=720)	OS				PFS			
			Outcome (death)	Average survival (month)	χ^2	P value	Outcome (recurrence)	Average survival (month)	χ^2	P value
TIL-T	T-low	199 (27.6)	8 (12.5)	58.996	8.448	0.004	13 (16.9)	58	5.456	0.019
	T-high	521 (72.4)	56 (87.5)	56.447			64 (83.1)	55.528		
TIL-B	B-low	297 (41.2)	13 (20.3)	58.716	13.335	<0.001	18 (23.4)	58.049	12.107	0.001
	B-high	423 (58.8)	51 (79.7)	56.052			59 (76.6)	54.914		
TIL	TIL-low	377 (52.4)	11 (17.2)	59.243	36.497	<0.001	21 (27.3)	58.353	23.651	<0.001
	TIL-high	343 (47.6)	53 (82.8)	54.843			56 (72.7)	53.839		

ccRCC, clear cell renal cell carcinoma; OS, overall survival; PFS, progression-free survival; TIL, tumor-infiltrating lymphocyte; TLS, tertiary lymphoid structure; TNM, tumor node metastasis; WHO/ISUP, WHO/International Society of Urologic Pathologist.

of 900 and requiring experimental evidence. Due to the large number of genes, the building option was set to zero order. The TF-gene interaction database employed TRRUST, a curated database of human transcriptional regulatory network. The gene set variation analysis (GSVA) R package was applied to estimate pathway activity scores in the cell populations.

Calculation of senescence scores

To quantify the underlying cell senescence in ccRCC microenvironment, we used the VISION V.2.1.0 R package to annote variations and calculate senescence scores based on directions provided on Github (https://www.github.com/ YosefLab/VISION).[22] The gene signatures in the senescence module were obtained from the CellAge Database (https://genomics.senescence.info/cells).[23]

SSIGN and Leibovich score

Composite scoring systems (Mayo Clinic stage, size, grade, and necrosis (SSIGN) and Leibovich score)) were constructed for prognostic stratification. SSIGN score which incorporates these several pathologic features demonstrated discriminative accuracy and was proved to compare favorably with TNM stage.[24 25] The scores were evaluated to remain as useful prediction tools with external validations in current clinical practice.[26 27]

Statistical analysis

The sample size was determined based on the primary endpoint using the log-rank test through Power and Sample Size Calculators (http://powerandsamplesize.com).[28] According to a previous study,[29] we assumed that the proportion of TLS-positive patients would be 30% and the HR would be 3. The overall probability of the event occurring within the study period was 0.068. With these assumptions, we calculated that a sample of 455 patients would provide the study with 80% power to identify survival distinction using a two-sided test at an α level of 0.05 (the number of patients we included is 720).

Statistical analysis of two-tailed Mann-Whitney U test or Student's t-test was performed for continuous variables, and χ^2 test or Fisher's exact test was conducted for categorical variables using IBM SPSS statistical software V.26. Receiver operating characteristics (ROC) analysis was conducted to determine the cut-off value and area under curve. Kaplan-Meier survival analysis and Cox regression analysis were performed using GraphPad Prism V.9.4.0 (GraphPad Software). Log-rank test was applied to detect significance. All tests were two-sided. p<0.05 was defined as statistically significant. Prognostic accuracy of clinical factors was measured through Harrell's concordance index (c-index) analysis using "survcomp" package in R software V.4.0.0. Forest model was conducted by "forestmodel" (V.0.6.2) package. The nomogram was constructed based on the results of the multivariate Cox regression model using "foreign" (V.0.8–82) and "rms" (V.6.2–0) packages to establish the risk prediction model.

RESULTS

Identification and cellular composition of TLSs in ccRCC

A total of 720 patients were enrolled in the study. Lymphoid aggregate clusters were first identified in all the patients by primary screening the H&E slides. To further confirm the structures of TLSs, we identified lymphocyte cell clusters with a given marker through IHC-stained sessions. TLSs were characterized by $CD20^+$B cell aggregates surrounded by $CD3^+$T cell clusters, forming a dense immune intense zone (figure 1A,B). Among all the 720 ccRCC patients involved in our study, 192 intratumoral TLSs were detected in the tumor samples of 113 ccRCC patients (16%, 113/720) (online supplemental table S1). Six types of immune cells including T helper (Th) cells ($CD3^+CD4^+$), cytotoxic T lymphocytes ($CD3^+CD8^+$), GC B cells ($CD20^+CD21^+$), natural killer (NK) cells ($CD56^+$), M1 macrophages ($CD68^+CD163^-$), M2 macrophages ($CD68^+CD163^+$) were presented in the ccRCC tumor tissues. Although B and T cell populations made up the bulk of TLS-related immune cells in both mature and immature TLSs, different shapes and structures were also observed in these areas. Representative H&E and mIF images of intratumoral TLSs in ccRCC patients displayed the heterogeneity of TLSs within tumor tissues. In mature TLSs, GC B cells were intensely clustered in the central area while Th cells and cytotoxic T lymphocytes were scattered in the peripheral regions. Mature TLSs are also populated with small proportions of macrophages and NK cells (figure 2). In line with previous research,[30] mature TLSs exhibited upregulated enrichment of vascularization, which mediates lymphocytes homing and infiltration into tumors (figure 2). These observations further validate the assessment of TLS maturity stratification.

Features of TLSs correlate with prognostic value of ccRCC

To evaluate the abundance of TLSs within a given tumor, all TLSs were divided by the tumor area to represent its density (figure 1C). Of all TLS-positive tumors, the median TLS density was 0.6/mm^2. Using this cut-off value, the 113 patients with intratumoral TLSs were classified into a low-density group and a high-density group to investigate the effect of TLSs on patient survival. The result of Kaplan-Meier analysis displayed that high-density of TLSs was associated with a better OS and PFS (figure 1D, online supplemental figure S2A). The survival differences relative to the clinicopathological parameters are shown in online supplemental figure S1.

Considering that the effect of TLSs on tumor control may be associated with intra-TLS immune cells, we further enumerated the inner immune infiltrates within TLS the region. We found that the local density and proportion of B cells within TLSs were clinically significant. The characteristic of B cells may be informative to discriminate occurrence for patients. Indeed, B cells were less abundant with lower density (defined as the ratio of B cell number to the area of the TLSs region) within TLSs in patients who experienced relapse after surgery (figure 1E). Similarly, the proportion of CD20+B cells within the TLSs region were higher in favorable than poor outcome group. (figure 1F).

According to the maturity score mentioned in the methods section, the median maturation score was 1.8. Using this cut-off value, patients with TLSs were divided into less mature TLS and mature TLS groups. Kaplan-Meier survival curve showed that mature TLSs predicted a better prognosis in ccRCC patients (figure 1G, online supplemental figure S2B). The correlation between TLS maturity and clinical characteristics is shown in online supplemental table S2.

High expression of TILs as a predictor of poor prognosis in ccRCC patients

The $CD3^+$T and $CD20^+$B immune infiltrates were evaluated with continuous IHC score as described in the methods section. We observed that the expression of intratumoral TILs differed in a considerable portion of samples (figure 3A,B). The diagnostic criteria to assess the TIL presence were inferred from the training cohort and validated with an independent set of tumors for TIL-T, TIL-B, TIL. ROC curve demonstrated that the optimal cut-off value was 74.5 for TIL-T, 59.5 for TIL-B, and 151 for TIL (figure 4A,B). Subsequently, the prognostic value was assessed in the testing cohort. Kaplan-Meier analysis showed that the survival was different in patients with different intensities of TIL infiltration. The same tendency indicated that higher intratumoral lymphocyte infiltration predicted worse OS and PFS in ccRCC (figure 4C,D, online supplemental figure S2C,D). Higher expressions of TILs were detected in individuals with bad outcomes as compared with those with good outcomes (figure 4E). And the expressions of T and B cells were strongly correlated in ccRCC tissues (figure 4F) with a Pearson's correlation coefficient of 0.742. Initial investigations to determine the clinical relevance showed that TIL-high group was substantially correlated with high WHO/ISUP grade (p<0.001), advanced stage (p=0.003) and T stage (p=0.002), necrosis (p=0.049), PFS (p<0.001) and OS (p<0.001) (online supplemental table S4–S6). TIL was shown as influencing factors of patient survival (table 1).

Prognostic models and stratified analysis of ccRCC patients

Cox regression analysis was performed to determine the predictive factors of OS and PFS (figure 5A, online supplemental figure S3A). Univariate analysis showed that the following features were associated with an increased death risk: old age (p<0.001), WHO/ISUP grades III and IV (p<0.001), TNM grades 3 and 4 (p<0.001), T3 and T4 (p<0.001), necrosis (p<0.001), cystic architecture (p=0.044), multifocality (p<0.001), size (p<0.001), high density of TIL-T (p=0.009), high density of TIL-B (p=0.001), and high density of TIL (p<0.001). After multivariable adjustment, TIL (HR=4.468, p<0.001), age (HR=1.038, p=0.002), WHO/ISUP grade (HR=1.895, p=0.032), and size (HR=2.375, p=0.006) were retained as independent risk factors of OS in ccRCC patients

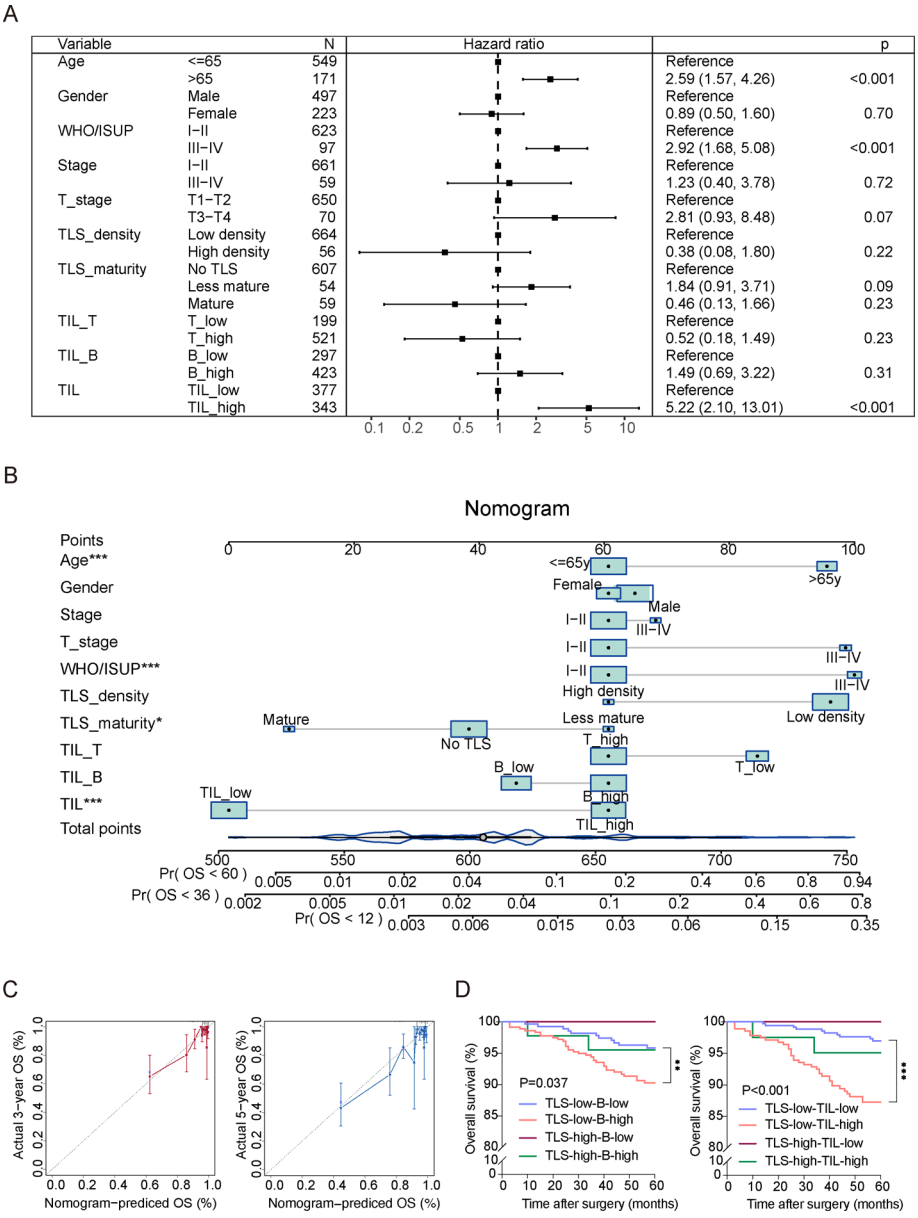

Figure 5 The immune infiltration and clinical characteristics predict the OS of ccRCC patients. (A) Forest plot of the effect of patient characteristics on OS by subgroup; (B) Nomogram for predicting OS at 1, 3 or 5 years after surgery; (C) Calibration plots of the nomogram for predicted and actual results of 3 years and 5 years OS; (D) Kaplan-Meier survival curves of TLS-B cell density (p=0.037) and TLS-TIL density (p<0.001) with clinical outcome. *p<0.05; **p<0.01; ***p<0.001. ccRCC, clear cell renal cell carcinoma; OS, overall survival; TILs, tumor-infiltrating lymphocytes; TLSs, tertiary lymphoid structures.

(table 2). Finally, we constructed nomograms based on the clinical information, TILs and TLSs to predict OS (figure 5B) and PFS (online supplemental figure S3B) of ccRCC patients. The calibration plots of 3-year and 5-year OS and PFS of the nomograms are presented in figure 5C and online supplemental figure S3C. Taken together, the proportion of intratumoral TILs was identified as an independent risk factor for OS of ccRCC patients. These results illustrated the significance of immune infiltrates as potential valuable predictive and prognostic factors of ccRCC.

Given the complementary roles in the immune contexture, we next explored the prognostic effect with the correlation between intratumoral TLSs and TILs. According to the density of TLSs and TILs, individuals were divided into four groups: TLS-low-TIL-low, TLS-low-TIL-high, TLS-high-TIL-low, and TLS-high-TIL-high. The combined indicators showed better stratification of the survival. The group with low expression of TLSs and high expression of TILs showed the worst OS and PFS (figure 5D, online supplemental figure S3D). Additionally, in the TLS-low subgroups, elevated B cell or TIL expressions were highly linked to poor outcomes (OS: p<0.001; PFS: p=0.003). The correlations between TLS-TIL expression and pathological characteristics displayed discrepancy in WHO/ISUP grade, OS and PFS (online supplemental tables S7–S10).

Table 2 Univariate and multivariate Cox regression analysis of patient characteristics with overall survival in the naïve cohort (n=720)

Characteristics, n (%)		Total (n=720)	Univariate HR (95% CI)	P value	Multivariate HR (95% CI)	P value
Age		720	1.047 (1.025 to 1.070)	**<0.001**	1.038 (1.014 to 1.063)	**0.002**
Gender						
	Male	497 (69)	Reference		Reference	
	Female	223 (31)	0.737 (0.419 to 1.298)	0.291	0.807 (0.443 to 1.471)	0.483
WHO/ISUP grade						
	I and II	623 (86.5)	Reference		Reference	
	III and IV	97 (13.5)	6.067 (3.707 to 9.929)	**<0.001**	1.895 (1.056 to 3.400)	**0.032**
TNM stage						
	1 and 2	661 (91.8)	Reference		Reference	
	3 and 4	59 (8.2)	7.078 (4.221 to 11.867)	**<0.001**	1.821 (0.496 to 6.685)	0.366
T stage						
	T1 and T2	650 (90.3)	Reference		Reference	
	T3 and T4	70 (9.7)	7.175 (4.338 to 11.868)	**<0.001**	1.466 (0.406 to 5.302)	0.559
Necrosis						
	Absent	598 (83.1)	Reference		Reference	
	Present	122 (16.9)	3.868 (2.355 to 6.354)	**<0.001**	1.456 (0.818 to 2.592)	0.201
Sarcoma						
	Absent	712 (98.9)	Reference		Reference	
	Present	8 (1.1)	3.182 (0.778 to 13.010)	0.107	1.142 (0.233 to 5.600)	0.870
Cystic architecture						
	Absent	581 (80.7)	Reference		Reference	
	Present	139 (19.3)	0.421 (0.182 to 0.975)	**0.044**	0.438 (0.186 to 1.034)	0.059
Multifocality						
	Absent	695 (96.5)	Reference		Reference	
	Present	25 (3.5)	4.531 (2.160 to 9.506)	**<0.001**	2.267 (0.973 to 5.284)	0.058
Size						
	≤4 cm	464 (64.4)	Reference		Reference	
	>4 cm	256 (35.6)	4.559 (2.666 to 7.793)	**<0.001**	2.375 (1.283 to 4.397)	**0.006**
TLS density						
	Low density	664 (92.2)	Reference		Reference	
	High density	56 (7.8)	0.377 (0.092 to 1.543)	0.175	0.515 (0.103 to 2.580)	0.420
TLS maturity						
	Less mature	661 (91.8)	Reference		Reference	
	Mature	59 (8.2)	0.556 (0.174 to 1.770)	0.320	0.425 (0.110 to 1.633)	0.213
TIL-T						
	T-low	199 (27.6)	Reference		Reference	
	T-high	521 (72.4)	2.856 (1.361 to 5.991)	**0.006**	0.579 (0.210 to 1.597)	0.291
TIL-B						
	B-low	297 (41.2)	Reference		Reference	
	B-high	423 (58.8)	2.947 (1.603 to 5.419)	**0.001**	2.071 (0.988 to 4.341)	0.054
TIL						
	TIL-low	377 (52.4)	Reference		Reference	
	TIL-high	343 (47.6)	5.836 (3.048 to 11.175)	**<0.001**	4.468 (1.812 to 11.018)	**<0.001**

Continued

Table 2 Continued

Characteristics, n (%)	Total (n=720)	Univariate HR (95% CI)	Univariate P value	Multivariate HR (95% CI)	Multivariate P value

P value <0.05 is marked in bold.
ISUP, International Society of Urologic Pathologist; TIL, tumor-infiltrating lymphocyte; TLS, tertiary lymphoid structure.

Additionally, the evaluation of TLSs showed an added discriminatory ability in SSIGN and Leibovich scores for risk stratification in ccRCC. We discovered that patients with the same risk groups could be stratified into different risk groups based on dichotomized immune infiltration characteristics (online supplemental figure S4A–F). This was primarily evident among patients with low-risk and intermediated-risk disease, which led to more personalized treatment for ccRCC patients. In the concordance index analysis, the SSIGN and Leibovich models showed improved prognostic accuracies when integrated with TLS features in all data sets (table 3). TILs presented an advantageous value in combination with clinical staging systems (online supplemental table S11).

The roles of TLS and TIL infiltrations of ccRCC in response to first-line treatment

A cohort of patients who received first-line TKI or combination therapy were evaluable for response. Baseline characteristics of patients are summarized in table 4. We investigated typical TLS regions in the tumor tissues and compared different TLSs presence in both responders and non-responders (figure 6A). The analysis of TLS characteristics revealed that tumors that responded to therapy exhibited significantly higher TLS density (p<0.001) and maturity scores (p=0.02) compared with non-responsive tumors (figure 6B). TLS-positive cases showed positive responsiveness to the combination treatment. Patients with mature TLSs exhibited the highest response rate after treatment. We subsequently investigated the B and T lymphocyte infiltrations and found that high infiltration of TILs predicted worse PFS in patients undergoing treatment (online supplemental figure S4G). Therefore, our data indicate that the TLS states and features in combination with TILs are associated with the response to treatment and prognosis of ccRCC patients. Furthermore, Kaplan-Meier curve showed that the presence of TLSs predicted better PFS following first-line treatment administrations (p=0.002, figure 6C).

Combination of age and TLSs predicts the clinical outcome of ccRCC patients

The multivariate Cox analysis showed that old age and high-density TILs were factors significantly associated with dismal OS. However, little was known about the possible synergistic effect of intratumoral immune infiltrates and age in predicting the prognosis of ccRCC. Given the common association of malignancies with both chronic inflammation and aging,[31 32] we hypothesized the existence of age-dependent TLS formation or local immune dysfunction mechanisms in age-related kidney diseases. Kaplan-Meier survival curve displayed a significant survival difference in terms of OS and PFS between the four groups (figure 7A, online supplemental figure S4H). We found that old-immature group had the worst outcome (figure 7B, online supplemental figure S4I). Subgroup analysis showed that among individuals with immature TLSs, younger patients had a better survival rate than older patients. Then, we validated our findings in TCGA-KIRC cohorts. The Kaplan-Meier survival curve showed that the prognosis was worse in old-TLS low and old-immature TLS groups (figure 7C). Using CD21 expression as the marker of mature TLSs, we found that the mean CD21 expression level in older patients was lower than that in younger

Table 3 Concordance index analysis of the prognostic accuracy of TLS and prognostic models for overall survival in the naïve cohort (n=720)

Characteristics	Overall survival	Progression-free survival
SSIGN score (0–5 vs ≥6)*	0.6370 (0.5812–0.6928)	0.6342 (0.5837–0.6846)
Leibovich score (0–5 vs ≥6)*	0.6399 (0.5846–0.6952)	0.6333 (0.5832–0.6834)
TLS density (low vs high)	0.5230 (0.4992–0.5468)	0.5286 (0.5101–0.5470)
TLS maturity (immature vs mature)	0.5195 (0.4948–0.5441)	0.5175 (0.4934–0.5416)
SSIGN+TLS_density	0.6546 (0.5995–0.7098)	0.6558 (0.6075–0.7041)
SSIGN+TLS_maturity	0.6432 (0.5839–0.7024)	0.6386 (0.5840–0.6931)
Leibovich+TLS_density	0.6579 (0.6033–0.7124)	0.6557 (0.6078–0.7035)
Leibovich+TLS_maturity	0.6463 (0.5876–0.7050)	0.6382 (0.5840–0.6924)

*For clinical application, SSIGN and Leibovich score were defined as low risk (scores 0–2), intermediate risk (3–5), and high risk (6 or higher).
SSIGN stage, size, grade, and necrosis; TLS, tertiary lymphoid structure.

Table 4 Baseline characteristics for patients with first-line therapy in the treatment cohort (n=34)

Characteristics	Value
Age at nephrectomy (years)	
Mean±SD	58.2±11.4
Median	58
Range	25–77
Gender	
Male	23 (67.6%)
Female	11 (32.4)
Primary tumor status (pathologic TNM stage)*	
I	7 (20.6%)
II	0
III	12 (35.3%)
IV	15 (44.1%)
Progression-free survival (months)	
Mean±SD	18.7±19.0
Median	10.3
Range	1–65

*According to 2010 American Joint Committee on Cancer TNM staging.

patients (figure 7D). Together, these data suggest that age-associated intratumoral immune infiltrates could predict clinical prognosis of ccRCC, and the mechanisms between aging and immune alteration needs further investigation.

Transcriptomic analysis of TLS heterogeneity in ccRCC

To study the population of immune cells in the TME at single cell resolution, we isolated activated cells from fresh tumor tissues of 15 patients who were pathologically diagnosed with ccRCC, and retrieved transcriptional information of 6 patients from previous study. After initial quality filtering and batch effect correction, we obtained 140,804 single cells for further analysis, which were classified into eight clusters according to the marker genes, including tumor cells, endothelial cells, myeloid cells, T_NK cells, tubules, fibroblasts, B cells and proliferative cells (figure 7E). To interrogate TLS heterogeneity, we initially focused on B cell lineage and generated a profile for B and plasma subclusters via uniform manifold approximation and projection. Based on distinct lineage markers, 1294 single B lineage cells were further separated into six major clusters, including activated B cells, immature B cells, plasma cells, plasmablast-like cells, follicular B cells and GC B cells (figure 7F). Signature genes in B cell subgroups were presented in the heatmap (figure 7H). The volcano plot showed the DEGs between the old and young (figure 7I). The PPI network is shown in online supplemental figure S6.

scRNA-seq analysis of TLS aging in human ccRCC

As the main components of TLSs, B-cell development stages were broadly outlined.[33 34] GC within the TLSs contains rapidly proliferating cells serving as the main site for B cell maturation into plasma cells. Fully mature TLSs displayed active GC reaction with plasmablast-like cells, plasma cells and GC B cells. To interrogate cellular senescence score, we analyzed hallmark genes using CellAge Database using Vision (figure 7G). Besides, the senescence score among immune cell groups ranked high in the elderly (figure 7J). This suggests that age-associated changes in immune components could contribute to the immunosenescence and dysfunction in the ccRCC microenvironment. Specifically, in the context of B cells, the average senescence score in the old group is 1.53 times higher compared with the young group. Similarly, for T and NK cells, the ratio is 1.19, and for myeloid cells, it is 1.15. Significant variations in senescence scores were observed among different groups ($p<0.001$) (online supplemental figure S7A). To identify signaling pathways associated with TLS cell components, GSVA was performed to identify biological features in ccRCC patients. We calculated the pathway activity scores in both young and old groups. It was found that aging-associated pathways scored high in the old group (figure 7K,L) while immune response was lower in older individuals (online supplemental figure S7A–C). Additionally, this analysis highlighted the advanced differentiation state, reduced stem cell properties and DNA replication in older groups (online supplemental figure S7D–K). We speculated that that immune cell senescence may be associated with TLS maturation states, which might act as a springboard for future mechanistic study of the immune landscape with aging in tumor growth.

DISCUSSION

We provided a detailed assessment of the clinical significance of immune infiltration within the ccRCC microenvironment. Among all the tissues, abundant and mature TLSs were associated with favorable survival and therapeutic benefit while high TILs infiltration predicted poor outcomes and response rates. In addition, immune senescence was first demonstrated in TLSs associated with age.

Compared with other malignancies,[16] a relatively low proportion of TLSs (16%) were identified in the ccRCC microenvironment. Different with a previous study,[29] we detected mature state TLSs with GC reaction in ccRCC. Continuous recruitment of B cells in GC diversify the immune response,[35] thus TLSs could serve the potential role of transforming an immune deserted phenotype into an immunogenic tumor. Actually, TLSs are the most plastic of lymphoid tissues,[36] whose formation could be internally or externally stimulated.[37–39] Markers of TLSs were increased in clinical trial of lung cancer patients with ipilimumab and nivolumab.[40] It is conceivable to exploit

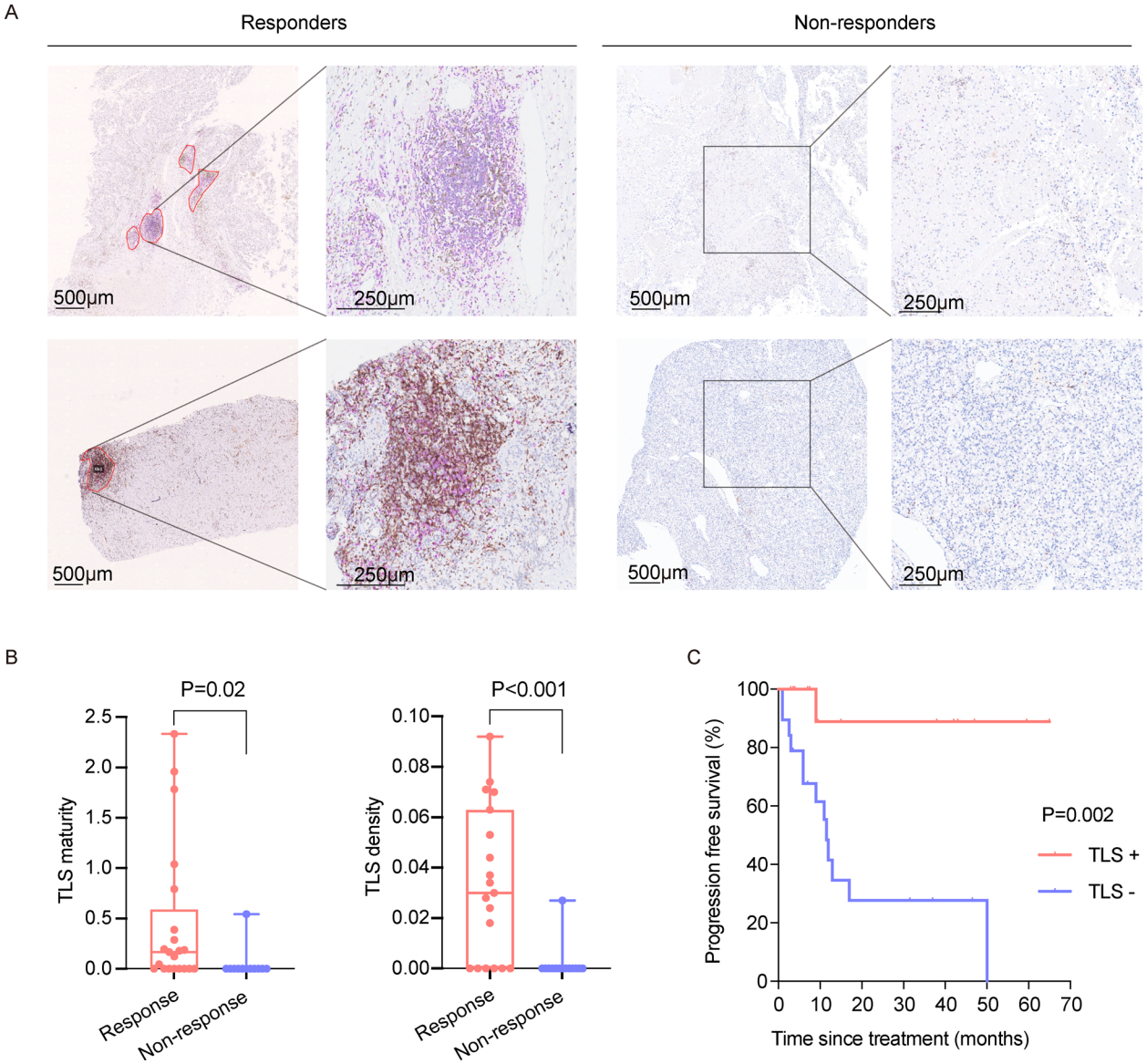

Figure 6 The correlation between TLSs and response to first-line TKI+IO combination therapies of ccRCC. (A) Representative figures of distinct TLSs expression in responders and non-responders to treatment of ccRCC. Scale bar, 500 μm and 250 μm; (B) TLS maturity (p=0.02) and density (p<0.001) in response and non-response groups; (C) Kaplan-Meier survival curve shows progression-free survival in TLS+and TLS- patients (p=0.002). ccRCC, clear cell renal cell carcinoma; IO, immunotherapy; TKI, tyrosine kinase inhibitor; TLSs, tertiary lymphoid structures.

therapeutic agents such as chemokines, antibodies or synthetic scaffolds combining with immunotherapies to modulate TLSs by increasing TLS numbers, shifting towards more mature TLSs and boosting TLSs function in ccRCC. Here, for the first time, we evaluated the association between TLSs and therapeutic response to the first-line treatment in large ccRCC cohorts.

Recent studies have illustrated the heterogeneous landscape of TLSs and TILs in distinct cancer types. Specifically, high density of TILs as well as the presence of TLSs were shown to predict coordinated and favorable predictive and prognostic effects in several cancers.[17 41 42] Conversely, we displayed significant differences in the roles of intratumoral TILs and TLSs in the clinical relevance and therapeutic response of ccRCC. The paradoxical outcome of effective responsiveness stressed the intricate and unique immune regulations in the ccRCC microenvironment. An adverse effect of $CD8^+$T cells in ccRCC has been indicated in contrast with most other malignancies.[43] The state of T cell exhaustion lead to the impairment or anergia of effector function and could be differentially remodeled by ICB treatment.[44 45] Furthermore, investigations into advanced ccRCC have unveiled the co-occurrence of terminally exhausted $CD8^+$T cells and suppressive M2-like macrophages, expressing specific inhibitory markers and associated with poor prognosis in ccRCC.[44] These bidirectional inhibitory interactions form a progressive immune dysfunction in the TME.[46] The intricate interplay was assumed to interrelate with the immunoevasive contexture in the ccRCC microenvironment, accompanied by

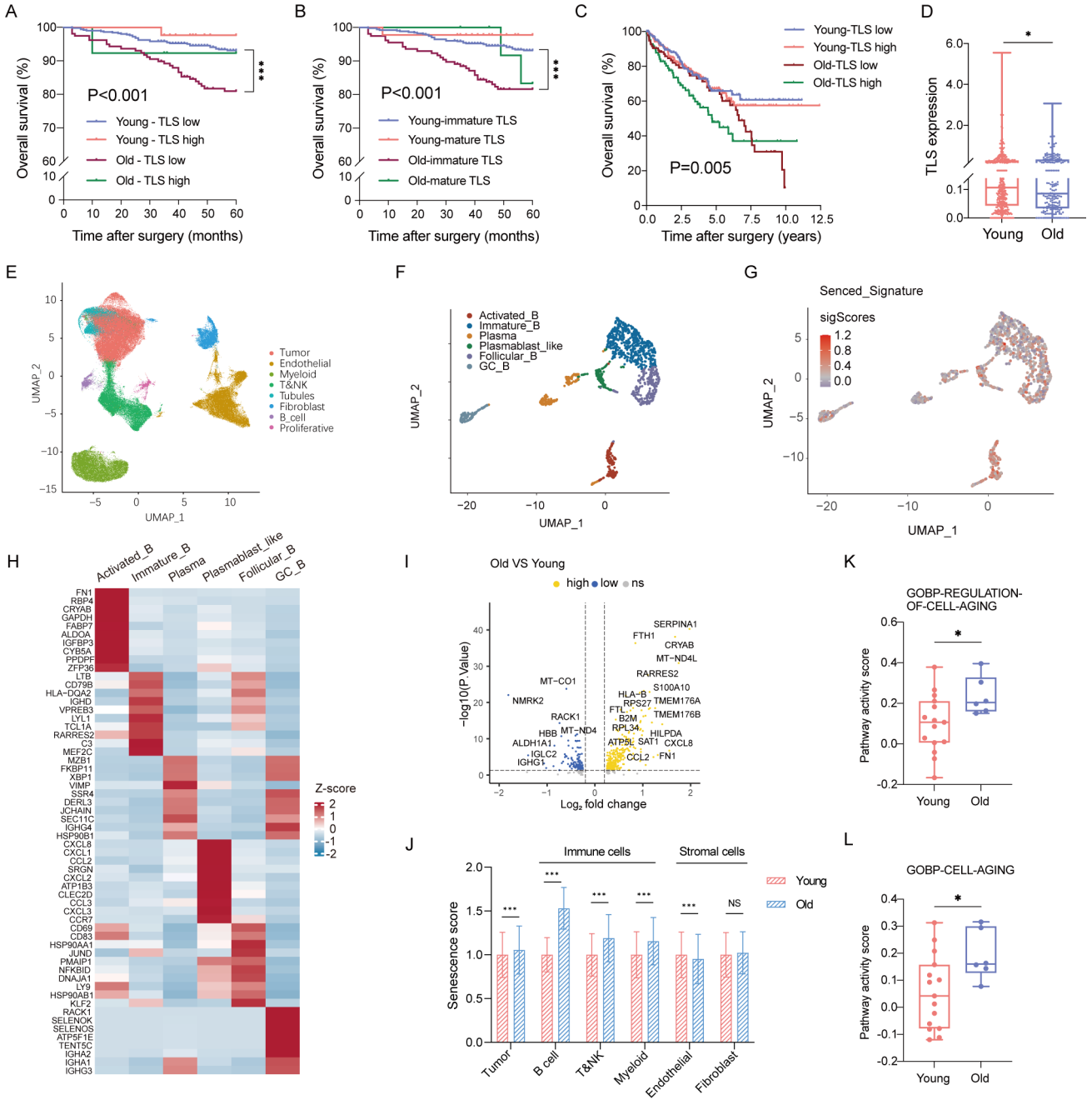

Figure 7 Age-related survival analysis and scRNA-seq analysis of TLS aging. (A) Kaplan-Meier survival curve of age-TLS density and clinical prognosis (p<0.001); (B) Kaplan-Meier survival curve of age-TLS maturity and clinical prognosis (p<0.001); (C) Kaplan-Meier survival curve of age-TLS density in TCGA dataset (p=0.005); (D) TLS expression level in young and old groups; (E) UMAP plot showing eight major cell clusters after Harmony treatment of the scRNA-seq datasets; (F) UMAP plot showing six major B cell subgroups; (G) UMAP plot showing senescence scores of B cells; (H) Heatmap showing the signature genes in B cell subgroups; (I) Volcano plot showing the differentially expressed genes between old and young groups in B cell cluster; (J) Statistics of senescence scores in young and old groups among all subsets; (K–L) Pathway activity scores of aging in young and old groups. UMAP, uniform manifold approximation and projection. *p<0.05; ***p<0.001. scRNA-seq, single cell RNA-sequencing; TCGA, The Cancer Genome Atlas; TLS, tertiary lymphoid structure; UMAP, uniform manifold approximation and projection.

increased myeloid-derived suppressor cells and decreased NK cells.[47] Besides, NK cell dysfunction has been verified in various tumors which may cause resistance to innate antitumor immune response.[48] Changes in the immune milieu in ccRCC could attenuate NK-mediated killing and result in tumor progression.[49 50] Studies revealed that the degree of immune cell exhaustion showed dependency on their spatial localization.[51] We speculate that TLSs may affect immunological milieu by participating in recruiting, reactivating or reeducating effector T cells.[52] On the other hand, B cells within well-structured TLSs provide assistance for T cells and indicate issues of

synergetic function[53] while B cells within poorly structured TLSs generate inhibitory factors that suppress the response of other immune cells.[15] We supposed that the different organization of immune infiltration—either dispersed or structured—resulted in the paradoxical properties of TLSs and TILs in ccRCC. Additionally, the cross-talk between TLSs and other components including tumor-associated macrophages also linked to tumor control in immunotherapy. Conclusively, the immune response and therapeutic effect in ccRCC patients are closely correlated with the quality and magnitude of TLSs and TILs.

Serendipitously, we discovered that the prognostic value of TLSs was stratified by age in ccRCC patients. Based on senescence-associated secretory phenotype,[54] we detected high senescence characteristics in both immature TLSs and aged patients at a single cell level. Indeed, age-induced immune subtype switching was observed driving tumor progression.[55] The coining of the term "Immunosenescence" emphasizes the aging of the immune system which exhausts the ability of immune cells to renew themselves.[56] Clinically, new cutting-edged immunotherapies are proved effective in aged patients,[57] but there are conflicting results coupled with a lack of large enrolled elder individuals. According to our results and previous literature, aging alters the ccRCC immune landscape, with immunosenescence may hampering the process of TLSs development.

Some limitations still need to be addressed. It was a retrospective study and the follow-up duration was not long enough in some patients. Besides, external validation has not been included now.

Our study provides the first evidence of integrated intratumoral TLSs and TILs in ccRCC. Mature TLSs and high density of TLSs were correlated with better clinical prognosis, whereas a high proportion of TILs led to poor outcomes. Besides, TLSs serve as a predictor for therapeutic response and also act as a protective factor of PFS in ccRCC patients. Our further analysis of single-cell transcriptomic datasets revealed that aging-related pathways were more active in elderly patients, whereas immune responses exhibited greater dynamics in the young group.

Author affiliations
[1]Department of Urology, Xinhua Hospital Affiliated to Shanghai Jiaotong University School of Medicine, Shanghai, China
[2]Department of Urology, The Third Affiliated Hospital of the Second Military Medical University, Shanghai, China
[3]Department of Urology, PLA Central Military Command General Hospital, Wuhan, Hubei, China
[4]Department of Urology, Changzhou No 2 People's Hospital, Changzhou, Jiangsu, China
[5]Department of Urology, Renmin Hospital of Wuhan University, Wuhan, Hubei, China
[6]Department of Urology, Wuxi No 2 People's Hospital, Wuxi, Jiangsu, China
[7]Department of Urology, The First Affiliated Hospital of the Second Military Medical University, Shanghai, China

Contributors Study concept and design: Y-QW, W-JC, WZ and X-WP. Acquisition of data: all authors. Analysis and interpretation of data: Y-QW, W-JC and K-QD. Statistical analysis: Y-QW, W-JC and WZ. Drafting of the manuscript: Y-QW and W-JC. Critical revision of the manuscript: WZ, X-WP, K-QD, W-JC and Y-QW. Obtaining funding: X-GC. Supervision: X-GC, X-WP and L-HW. Guarantor: X-GC.

Funding This work was sponsered by National Natural Science Foundation of China (No. 82330094, 82072806, 82173265); Leading health talents of Shanghai Municipal Health Commission (2022LJ002); Shanghai Rising-Star Program (23QC1401400); the Natural Science Foundation of Shanghai (23ZR1441300); Hospital Funded Clinical Research, Xin Hua Hospital Affiliated to Shanghai Jiao Tong University School of Medicine (21XHDB06).

Competing interests None declared.

Patient consent for publication Not applicable.

Ethics approval This study involves human participants and was approved by the institutional review board at Xinhua Hospital (XHEC-C-2021-145-1). Participants gave informed consent to participate in the study before taking part.

Provenance and peer review Not commissioned; externally peer reviewed.

Data availability statement Data are available in a public, open access repository. The raw data are available from Genome Sequence Archive of Human in the BIG Data Center, Chinese Academy of Sciences under Bioproject number PRJCA013742, accession HRA003614 (for C1, C2, C3, C4, C5, C6, C7, C8, C9, C10, C12), Bioproject number PRJCA026264, accession HRA007478 for (C11, C13, C14), Bioproject number PRJCA017313, accession HRA004711 (for C15) that are publicly accessible at https://bigd.big.ac.cn/gsa-human. Single cell RNA sequencing data from a previous study can be obtained from the Gene Expression Omnibus repository under accession GSE156632 (for C16, C17, C18, C19, C20, C21) that are publicly accessible at https://www.ncbi.nlm.nih.gov/geo.

ORCID iD
Xin-Gang Cui http://orcid.org/0000-0002-0920-9439

REFERENCES

1 Moch H, Cubilla AL, Humphrey PA, *et al*. The 2016 WHO classification of tumours of the urinary system and male genital organs-Part A: renal, penile, and Testicular tumours. *Eur Urol* 2016;70:93–105.
2 Barata PC, Rini BI. Treatment of renal cell carcinoma: current status and future directions. *CA Cancer J Clin* 2017;67:507–24.
3 Ljungberg B, Albiges L, Abu-Ghanem Y, *et al*. European Association of Urology guidelines on renal cell carcinoma: the 2022 update. *Eur Urol* 2022;82:399–410.
4 Nagtegaal ID, Quirke P, Schmoll H-J. Has the new TNM classification for colorectal cancer improved care? *Nat Rev Clin Oncol* 2011;9:119–23.
5 Bruni D, Angell HK, Galon J. The immune contexture and immunoscore in cancer prognosis and therapeutic efficacy. *Nat Rev Cancer* 2020;20:662–80.
6 Angell H, Galon J. From the immune contexture to the immunoscore: the role of prognostic and predictive immune markers in cancer. *Curr Opin Immunol* 2013;25:261–7.
7 Janssen LME, Ramsay EE, Logsdon CD, *et al*. The immune system in cancer metastasis: friend or foe? *J Immunother Cancer* 2017;5:79.
8 Galon J, Fridman W-H, Pagès F. The adaptive immunologic microenvironment in colorectal cancer: a novel perspective. *Cancer Res* 2007;67:1883–6.
9 Fridman WH, Zitvogel L, Sautès-Fridman C, *et al*. The immune contexture in cancer prognosis and treatment. *Nat Rev Clin Oncol* 2017;14:717–34.

10 Vanhersecke L, Brunet M, Guégan J-P, *et al*. Mature tertiary lymphoid structures predict immune checkpoint inhibitor efficacy in solid tumors independently of PD-L1 expression. *Nat Cancer* 2021;2:794–802.
11 Schumacher TN, Thommen DS. Tertiary lymphoid structures in cancer. *Science* 2022;375:eabf9419.
12 Helmink BA, Reddy SM, Gao J, *et al*. B cells and tertiary lymphoid structures promote immunotherapy response. *Nature* 2020;577:549–55.
13 Cabrita R, Lauss M, Sanna A, *et al*. Tertiary Lymphoid structures improve immunotherapy and survival in Melanoma. *Nature* 2020;577:561–5.
14 Petitprez F, de Reyniès A, Keung EZ, *et al*. B cells are associated with survival and Immunotherapy response in sarcoma. *Nature* 2020;577:556–60.
15 Bruno TC. New predictors for immunotherapy responses sharpen our view of the tumour microenvironment. *Nature* 2020;577:474–6.
16 Sautès-Fridman C, Petitprez F, Calderaro J, *et al*. Tertiary lymphoid structures in the era of cancer immunotherapy. *Nat Rev Cancer* 2019;19:307–25.
17 Kroeger DR, Milne K, Nelson BH. Tumor-infiltrating plasma cells are associated with tertiary Lymphoid structures, Cytolytic T-cell responses, and superior prognosis in ovarian cancer. *Clin Cancer Res* 2016;22:3005–15.
18 Meylan M, Petitprez F, Becht E, *et al*. Tertiary Lymphoid structures generate and propagate anti-tumor antibody-producing plasma cells in renal cell cancer. *Immunity* 2022;55:527–41.
19 Lau D, Lan LY-L, Andrews SF, *et al*. Low CD21 expression defines a population of recent germinal center graduates primed for plasma cell differentiation. *Sci Immunol* 2017;2:eaai8153.
20 Bankhead P, Loughrey MB, Fernández JA, *et al*. Qupath: open source software for Digital pathology image analysis. *Sci Rep* 2017;7:16878.
21 Zhang M, Zhai W, Miao J, *et al*. Single cell analysis reveals intra-tumour heterogeneity, microenvironment and potential diagnosis markers for clear cell renal cell carcinoma. *Clin Transl Med* 2022;12:e713.
22 DeTomaso D, Jones MG, Subramaniam M, *et al*. Functional interpretation of single cell similarity maps. *Nat Commun* 2019;10:4376.
23 Avelar RA, Ortega JG, Tacutu R, *et al*. A multidimensional systems biology analysis of cellular Senescence in aging and disease. *Genome Biol* 2020;21:91.
24 Leibovich BC, Blute ML, Cheville JC, *et al*. Prediction of progression after radical nephrectomy for patients with clear cell renal cell carcinoma: a stratification tool for prospective clinical trials. *Cancer* 2003;97:1663–71.
25 Frank I, Blute ML, Cheville JC, *et al*. An outcome prediction model for patients with clear cell renal cell carcinoma treated with radical nephrectomy based on tumor stage, size, grade and necrosis: the SSIGN score. *J Urol* 2002;168:2395–400.
26 Oza B, Eisen T, Frangou E, *et al*. External validation of the 2003 Leibovich Prognostic score in patients randomly assigned to SORCE, an international phase III trial of adjuvant sorafenib in renal cell cancer. *J Clin Oncol* 2022;40:1772–82.
27 Parker WP, Cheville JC, Frank I, *et al*. Application of the stage, size, grade, and necrosis (SSIGN) score for clear cell renal cell carcinoma in contemporary patients. *Eur Urol* 2017;71:665–73.
28 Chow S-C, Wang H, Shao J. *Sample Size Calculations in Clinical Research*. 2nd edn. 2008.
29 Masuda T, Tanaka N, Takamatsu K, *et al*. Unique characteristics of tertiary Lymphoid structures in kidney clear cell carcinoma: prognostic outcome and comparison with bladder cancer. *J Immunother Cancer* 2022;10:e003883.
30 Asrir A, Tardiveau C, Coudert J, *et al*. Tumor-associated high endothelial Venules mediate lymphocyte entry into tumors and predict response to PD-1 plus CTLA-4 combination immunotherapy. *Cancer Cell* 2022;40:318–34.
31 Niccoli T, Partridge L. Ageing as a risk factor for disease. *Curr Biol* 2012;22:R741–52.
32 Franceschi C, Campisi J. Chronic inflammation (Inflammaging) and its potential contribution to age-associated diseases. *J Gerontol A Biol Sci Med Sci* 2014;69 Suppl 1:S4–9.
33 LeBien TW, Tedder TF. B lymphocytes: how they develop and function. *Blood* 2008;112:1570–80.
34 De Silva NS, Klein U. Dynamics of B cells in germinal centres. *Nat Rev Immunol* 2015;15:137–48.
35 Hägglöf T, Cipolla M, Loewe M, *et al*. Continuous germinal center invasion contributes to the diversity of the immune response. *Cell* 2023;186:147–61.
36 Drayton DL, Liao S, Mounzer RH, *et al*. Lymphoid organ development: from Ontogeny to Neogenesis. *Nat Immunol* 2006;7:344–53.
37 Remark R, Lupo A, Alifano M, *et al*. Immune contexture and histological response after neoadjuvant chemotherapy predict clinical outcome of lung cancer patients. *Oncoimmunology* 2016;5:e1255394.
38 Morcrette G, Hirsch TZ, Badour E, *et al*. APC Germline Hepatoblastomas demonstrate cisplatin-induced Intratumor tertiary Lymphoid structures. *Oncoimmunology* 2019;8:e1583547.
39 Lutz ER, Wu AA, Bigelow E, *et al*. Immunotherapy converts nonimmunogenic pancreatic tumors into immunogenic foci of immune regulation. *Cancer Immunol Res* 2014;2:616–31.
40 Cascone T, Leung CH, Weissferdt A, *et al*. Neoadjuvant chemotherapy plus Nivolumab with or without Ipilimumab in operable non-small cell lung cancer: the phase 2 platform NEOSTAR trial. *Nat Med* 2023;29:593–604.
41 Wortman JC, He T-F, Solomon S, *et al*. Spatial distribution of B cells and lymphocyte clusters as a predictor of triple-negative breast cancer outcome. *NPJ Breast Cancer* 2021;7:84.
42 Di Caro G, Bergomas F, Grizzi F, *et al*. Occurrence of tertiary Lymphoid tissue is associated with T-cell infiltration and predicts better prognosis in early-stage colorectal cancers. *Clin Cancer Res* 2014;20:2147–58.
43 Giraldo NA, Becht E, Pagès F, *et al*. Orchestration and prognostic significance of immune checkpoints in the microenvironment of primary and metastatic renal cell cancer. *Clin Cancer Res* 2015;21:3031–40.
44 Bi K, He MX, Bakouny Z, *et al*. Tumor and immune reprogramming during immunotherapy in advanced renal cell carcinoma. *Cancer Cell* 2021;39:649–61.
45 Tsui C, Kretschmer L, Rapelius S, *et al*. MYB Orchestrates T cell exhaustion and response to checkpoint inhibition. *Nature* 2022;609:354–60.
46 Chakiryan NH, Kim Y, Berglund A, *et al*. Geospatial characterization of immune cell distributions and dynamics across the microenvironment in clear cell renal cell carcinoma. *J Immunother Cancer* 2023;11:e006195.
47 Dai S, Zeng H, Liu Z, *et al*. Intratumoral CXCL13+CD8+T cell infiltration determines poor clinical outcomes and Immunoevasive contexture in patients with clear cell renal cell carcinoma. *J Immunother Cancer* 2021;9:e001823.
48 Zhang P-F, Gao C, Huang X-Y, *et al*. Cancer cell-derived exosomal circUHRF1 induces natural killer cell exhaustion and may cause resistance to anti-PD1 therapy in hepatocellular carcinoma. *Mol Cancer* 2020;19:110.
49 Koh MY, Sayegh N, Agarwal N. Seeing the forest for the trees-single-cell Atlases link CD8+ T cells and Macrophages to disease progression and treatment response in kidney cancer. *Cancer Cell* 2021;39:594–6.
50 Tong L, Kremer V, Neo SY, *et al*. Renal cell carcinoma escapes NK cell-mediated immune surveillance through the downregulation of DNAM-1. *Cancer Communications* 2023;43:855–9.
51 Li R, Ferdinand JR, Loudon KW, *et al*. Mapping single-cell transcriptomes in the intra-tumoral and associated territories of kidney cancer. *Cancer Cell* 2022;40:1583–99.
52 Barone F, Gardner DH, Nayar S, *et al*. Stromal fibroblasts in tertiary Lymphoid structures: a novel target in chronic inflammation. *Front Immunol* 2016;7:477.
53 Wang Y-Q, Chen W-J, Li W-Y, *et al*. Impact of interaction networks of B cells with other cells on tumorigenesis, progression and response to immunotherapy of renal cell carcinoma: a review. *Front Oncol* 2022;12:995519.
54 Birch J, Gil J. Senescence and the SASP: many therapeutic avenues. *Genes Dev* 2020;34:1565–76.
55 Fane M, Weeraratna AT. How the ageing microenvironment influences tumour progression. *Nat Rev Cancer* 2020;20:89–106.
56 Rodrigues LP, Teixeira VR, Alencar-Silva T, *et al*. Hallmarks of aging and immunosenescence: connecting the dots. *Cytokine Growth Factor Rev* 2021;59:9–21.
57 Elias R, Hartshorn K, Rahma O, *et al*. Aging, immune Senescence, and immunotherapy: a comprehensive review. *Semin Oncol* 2018;45:187–200.